

Mercury Telluride Quantum Dot Based Phototransistor Enabling High Sensitivity Room Temperature Photodetection at 2000 Nanometers

Mengyu Chen^{1‡}, Haipeng Lu^{1‡}, Nema M. Abdelazim^{2‡}, Ye Zhu³, Zhen Wang⁴, Wei Ren⁴, Stephen V. Kershaw^{2}, Andrey L. Rogach², and Ni Zhao^{1*}*

¹Department of Electronic Engineering, The Chinese University of Hong Kong, Shatin, New Territories, Hong Kong S. A. R.

²Department of Physics and Materials Science and Centre for Functional Photonics (CFP) City University of Hong Kong, Hong Kong S. A. R.

³Department of Applied Physics, The Hong Kong Polytechnic University, Hong Kong S. A. R.

⁴Department of Mechanical and Automation Engineering, The Chinese University of Hong Kong, Shatin, New Territories, Hong Kong S. A. R.

*Stephen V. Kershaw. E-mail: skershaw@cityu.edu.hk,

*Ni Zhao. E-mail: nzhao@ee.cuhk.edu.hk

‡ these authors contributed equally to this work.

Supporting Information

1. Flow of ligand exchange process in solution. The intermediate product, DDT capped QDs, and final product, TG capped QDs, are made into thin films and examined by Fourier transform infrared spectroscopy (FTIR).

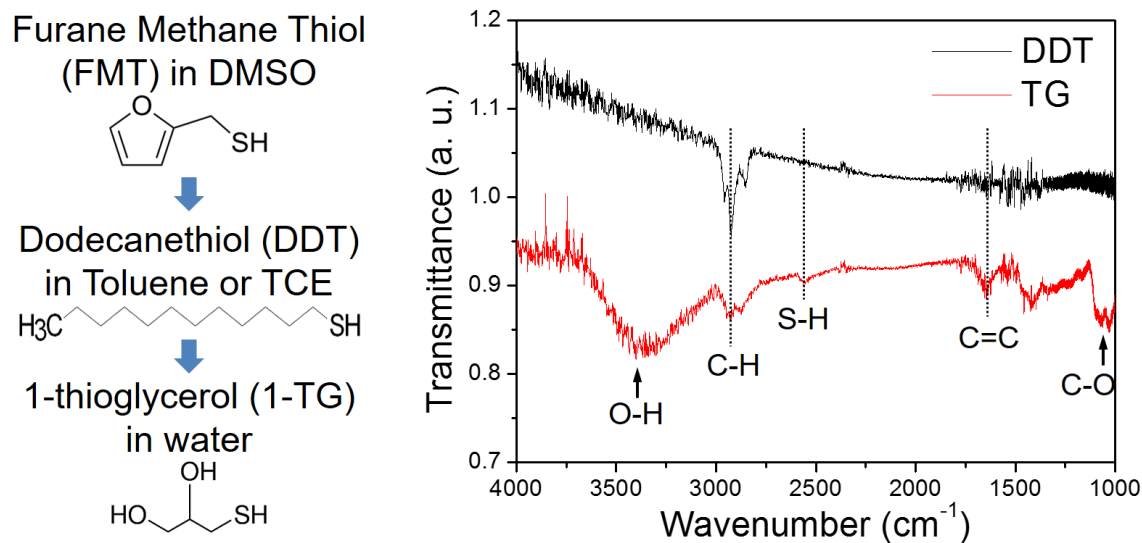


Figure S1. (Left) Solution phase ligand exchange process and the corresponding ligand structures used and (right) FTIR characteristics of the DDT and TG capped HgTe QDs in solid films.

Figure S1 shows the structures of different ligands associated with the solution-phase ligand exchange process of the HgTe QDs and the FTIR characteristics of the DDT and TG capped HgTe QDs in solid films. After the ligand exchange and wash-out process, the DDT capped HgTe QDs in toluene and the TG capped HgTe QDs in aqueous phase are directly drop-cast onto intrinsic silicon wafers for the FTIR measurement. The vibration peaks are marked with the possible chemical bonds¹, which correspond to the structures of different ligands.

For the DDT FTIR spectrum, the most obviously peak is the C-H bonds in the range from 2800 to 3000 wavenumber, which coincides with the dominant methylene and methyl structures in DDT. A very weak C=C bond vibration around 1650 wavenumber can also be observed, which could be attributed to the residual FMT or other impurities left after ligand

exchange. Considering that the C=C peak is much smaller than the C-H peak, the FTIR spectra appear to indicate that the ligand exchange from FMT to DDT is quite complete.

For the TG FTIR spectrum, the most obvious peak is a broad O-H band vibration from 2500 to 3600 wavenumber, which may come from the O-H group in TG and the residual water within the QD film. Note that the samples for the FTIR measurement were fabricated by directly drop-casting the solution onto the substrates and that no thickness calibration was performed. It is therefore not appropriate to directly compare the signal strength of the DDT and TG FTIR spectra to evaluate the extent of ligand exchange. However, since the amount of FMT residual within the TG-capped QD solution must be equal or less than that in the DDT-capped QD solution, we can use the C=C peak (characteristic signal from FMT) as the reference to evaluate the extent of ligand exchange from DDT to TG. Based on this assumption, the reduction of the C-H peak after the DDT-to-TG ligand exchange is evaluated to be more than 83%. At the same time, the C-O bond vibration around 1100 wavenumber rises up in the spectra, which can only be attributed to the existence of TG. It is also worth mentioning that the HgTe QDs can be well dissolved in aqueous solution after the DDT to TG ligand exchange, which would be hard to achieve if there is a lot of entrapped organic phase soluble DDT residue. All these observations support that the ligand exchange from DDT to TG is successful.

2. The transfer properties and the microscopic images of QD films with different numbers of spray passes.

The optical microscopy images in Figure S2 (b)-(f) reveal how the QD film morphology evolve with the increasing number of spray passes. Within the first 10 passes, the QD droplets start to connect with each other but do not fully cover the substrate. From 10 to 30 passes the

QDs start to fill up the voids while the QD film grows thicker. After 45 passes, the color of QD films gradually turns from green to dark brown. Through microscope observation, we note that the dark brown regions form due to resolving and redistribution of QDs during spray-coating, which often leads to poor film properties. The dark transfer characteristics of the aqueous HgTe QD based phototransistors also vary with the number of spray passes, as shown in Figure S2 (a). The trend is consistent with the film uniformity, *i.e.*, the gate effect is firstly enhanced with the spray passes from 10 to 30 and then gradually deteriorates after 45 passes. The conductivity of the QD films increases with the number of spray passes.

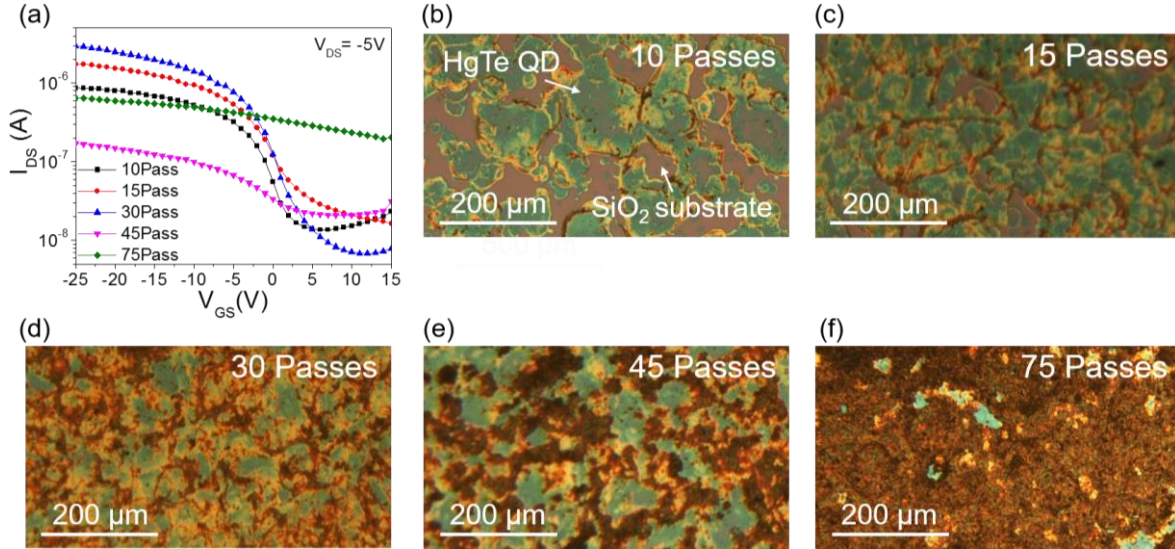


Figure S2. (a) Typical dark transfer characteristics of the aqueous HgTe QD based phototransistor fabricated with a range of spray passes (10 to 75). (b)-(f) Optical microscopy images of the QD film morphology with 10, 15, 30, 45 and 75 spray passes respectively.

3. Color-enhanced SEM images of the cross-sections of the spray-deposited aqueous HgTe QD films and the room-temperature absorption spectrum of the HgTe QD film.

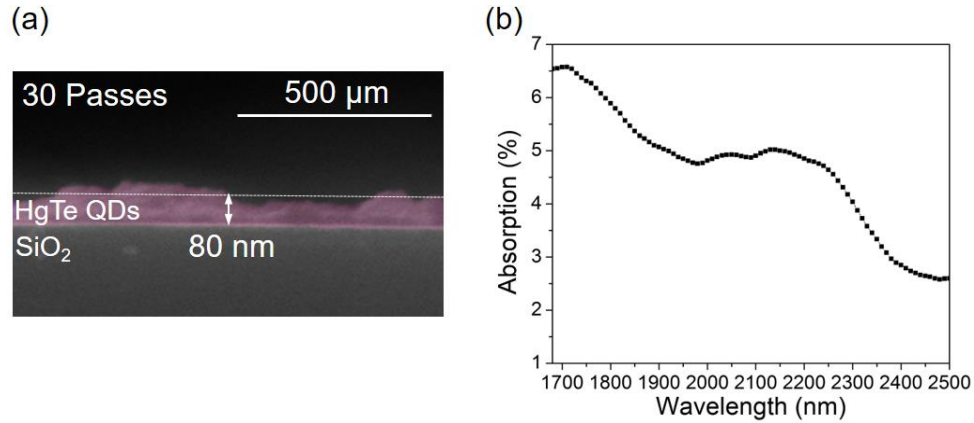


Figure S3. (a) Color-enhanced SEM images of the cross-sections of the spray-deposited aqueous HgTe QD films fabricated with 30 spray passes. (b) Room-temperature absorption spectrum of the HgTe QD film.

4. Leakage current

Figure S4 shows the dark and light transfer curves and the corresponding leakage current of the HgTe QD phototransistor (same device in Figure 2(b)).

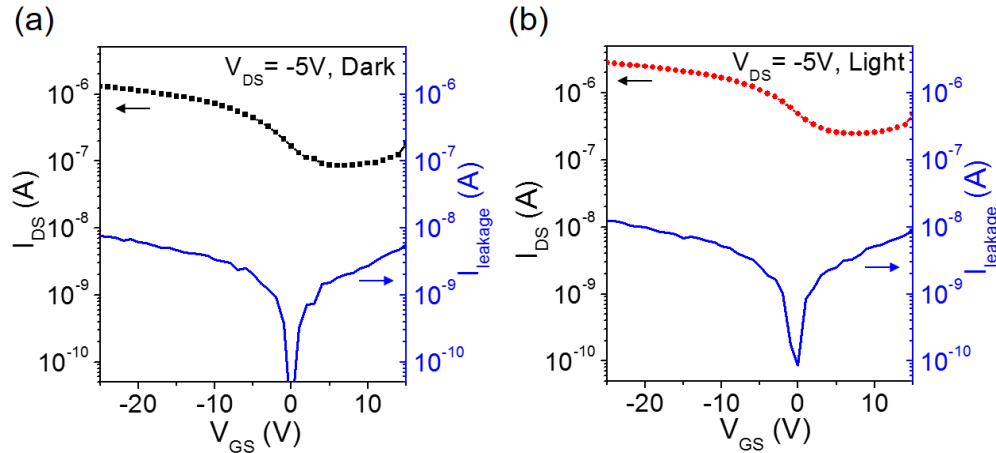


Figure S4. Dark (a) and light (b) transfer characteristics and the corresponding leakage currents of the HgTe QD based phototransistor (same device shown in figure 2(b)). Illumination level: 1550 nm, 4.2 mW/cm².

5. Ambipolar performance

The HgTe QD film supports ambipolar charge transport, as previously observed in other studies.^{2,3} The small n-type behavior at positive V_{GS} is a true n type behavior. The reason we

focused on the p-type region is because the p-type mobility ($1.40 \times 10^{-3} \text{ cm}^2/(\text{V}\cdot\text{s})$) is much higher than the n-type mobility ($3.97 \times 10^{-4} \text{ cm}^2/(\text{V}\cdot\text{s})$). We note that the electron transport may partially be suppressed by the RS^- groups from the negatively charged TG ligands or the OH terminated SiO_2 surface. To reduce trapping of electrons during transfer scans, we try to avoid electron injection in our device, therefore limiting the positive scan to below +15.

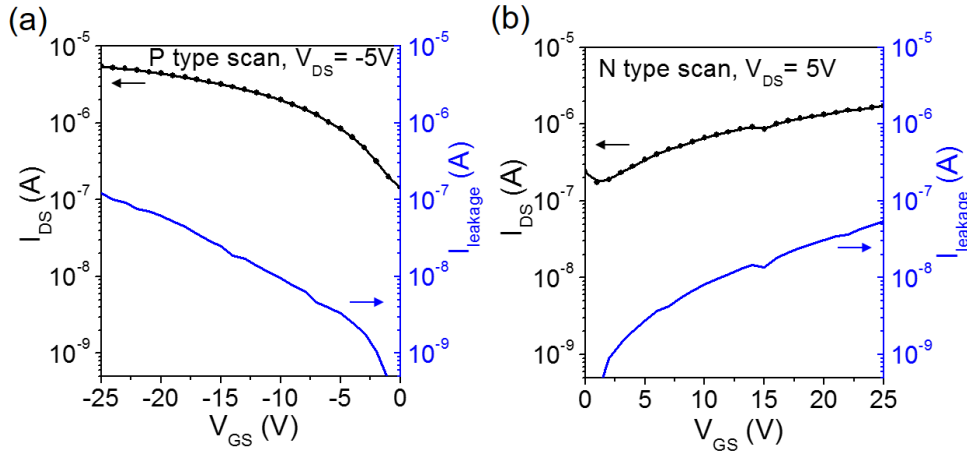


Figure S5. Dark transfer characteristics and the corresponding leakage currents of the HgTe QD based phototransistor (30 spray passes) in (a) p-type scan (scanning direction: 0V to -25V) and (b) n-type scan (scanning direction: 0V to 25V). All data are measured at 298 K.

6. Hysteresis of I-V curves.

Figure S6 shows the forward and reverse scans of a typical HgTe QD based phototransistor in dark. The device shows a relatively small hysteresis.

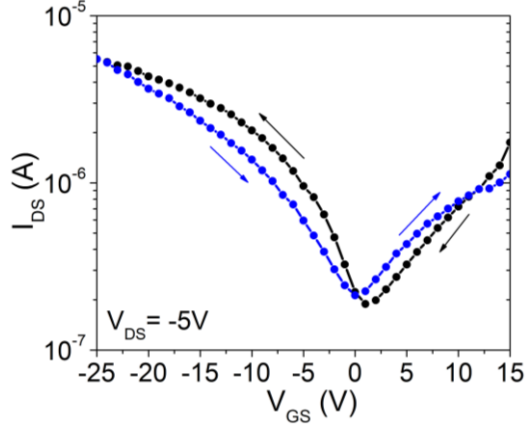


Figure S6. Backward (black) and forward (blue) scans of a typical HgTe QD based phototransistor (30 spray passes) under dark.

7. Evaluation of charge carrier density.

To evaluate the carrier density in accumulation mode, we take the general assumption that the charge carriers are located in the first QD monolayer.⁴ For $V_{GS} = -25V$, the charge carrier concentration is calculated to be $n_{charge} = C_{ox}(V_{GS} - V_{DS}/2 - V_T)/e = 1.98 \times 10^{12}$ charges/cm², where C_{ox} is the capacitance of gate oxide per unit area (11.5 nF/cm² in our case) and V_T is the threshold voltage (we use $V_T = 5V$). Charge density per QD (induced by the gate voltage) is evaluated to be ~ 0.49 charge per QD for QDs with a diameter of 5 nm. For depletion mode, we assume the current conduction is dominated by charge transport across the whole thickness of the bulk QD layer. Using $i = n\mu_h Ee$ (where i is the current density, n is the charge density, μ_h is the hole mobility, E is the source-drain electric field) and the current in depletion ($V_{ds} = -5V$, $V_{gs} = 6V$), we estimate the carrier density to be $\sim 5 \times 10^{15}$ charges/cm³, *i.e.* 6.5×10^{-4} charges per QD.

8. Light intensity dependence over a wide illumination range

A light intensity dependent measurement over a wide illumination range was performed. It can be clearly seen that at reduced illumination level the power law fitting between the photocurrent

(I_{ph}) and the illumination level (I) ($I_{ph} \propto I^\alpha$) is changed from α close to 0.5 to α close to 1, *i.e.* the linear response regime. At this range, the responsivity cannot be further increase by reducing the illumination level.

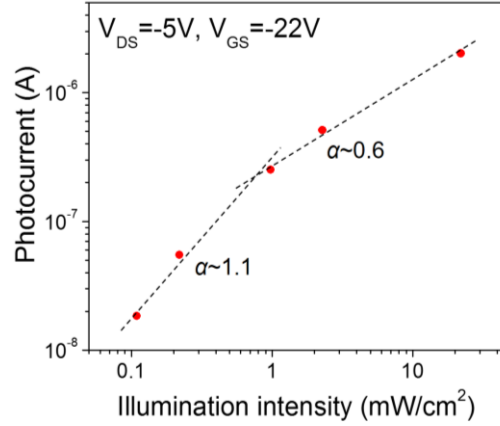


Figure S7. Light intensity dependence of photocurrent (dots) and log-log fit (dashed line) of a HgTe QD based phototransistor operated in the accumulation mode.

9. Noise measurement

Current noise level is measured by sealing the devices in a metal box with battery biased drain voltage and gate voltage (if not floating), in order to minimize the noise components from the environment and the bias sources. A lock-in amplifier (Stanford Research 830) is employed to measure the noise spectral density at different frequencies⁵. Figure S8 shows two possible noise measurement configurations where the lock-in amplifier is connected to our phototransistor in either series or parallel. In the series connected configuration (Figure S8(a)), the lock-in amplifier is operated in current input mode with the measurement unit A/Hz^{1/2}. The impedance of the lock-in amplifier in this mode is 1 kΩ, which is much smaller than the source-drain resistance of our device (larger than 1 MΩ even when a gate voltage was applied). That ensures

the accuracy of the measurement results. All the noise spectra we reported in this paper are measured in this configuration.

It should be noted that the current input to the lock-in amplifier should be no larger than $10\ \mu\text{A}$ and the internal noise current of the lock-in amplifier is $130\ \text{fA}/\text{Hz}^{1/2}$. In the larger input current and lower noise cases, the alternative configuration (Figure S8(b)) can be used, where a low-noise resistor is placed in parallel connection to the lock-in amplifier and the voltage across it was measured in voltage input mode. However, the noise level measured in this configuration is affected by the value of the resistor because of its action as a voltage divider and self-noise, which may introduce some inaccuracy.

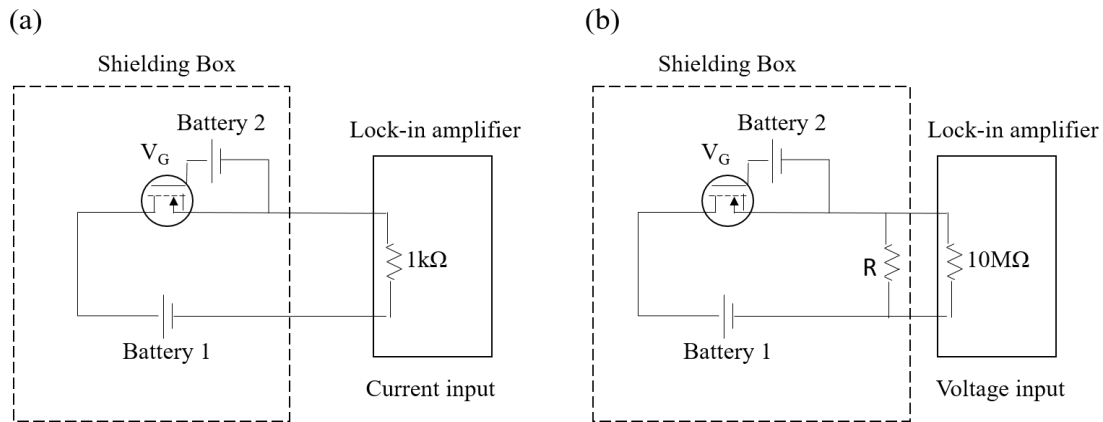


Figure S8. Schematic setups for noise measurement of our device with series (a) and parallel (b) connections to the lock-in amplifier.

10. Linear-scale dark transfer characteristics of the HgTe QD phototransistor (Figure 4(a)) at different temperatures and temperature dependent dark source-drain current of the same device.

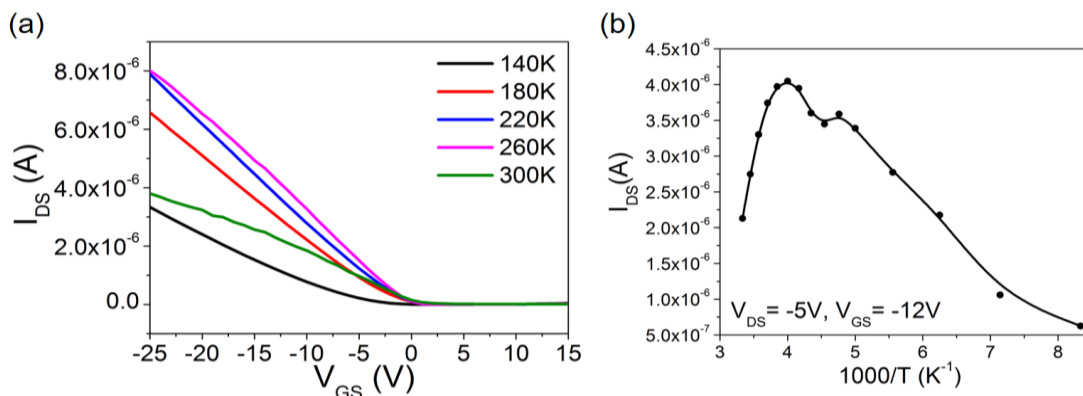


Figure S9. (a) Dark transfer characteristics of the HgTe QD phototransistor in a linear scale at different temperatures. (b) Dark source-drain current of the HgTe QD phototransistor as a function of temperature.

11. Reference absorption spectrum of CO gas at R(10) line.

Tunable diode laser absorption spectroscopy (TDLAS) is a typical technique for measuring the concentration of certain species.⁶ In our measurement, we used the absorption line of CO gas at 4297.7 cm^{-1} (R(10), about 2327 nm) based on the reference absorption spectrum (shown in Figure S10) calculated from the HITRAN database.

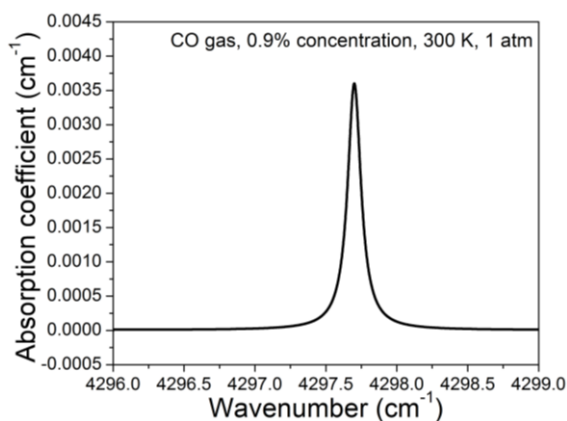


Figure S10. Absorption spectrum of CO gas at R(10) line under the measurement condition calculated from the HITRAN database.⁷

References

1. Griffiths, P. R. & de Haseth, J. A. *Fourier Transform Infrared Spectrometry*, John Wiley &

Sons. 2007; Ch. 10.

2. Chen, M., Yu, H., Kershaw, S. V., Xu, H., Gupta, S., Hetsch, F., Rogach, A. L. & Zhao, N. Fast, Air-stable Infrared Photodetectors Based on Spray-Deposited Aqueous HgTe Quantum Dots. *Adv. Funct. Mater.* **2014**, 24, 53–59.
3. Lhuillier, E., Keuleyan, S., Zolotavin, P. & Guyot-Sionnest, P. Mid-Infrared HgTe/As₂S₃ Field Effect Transistors and Photodetectors. *Adv. Mater.* **2013**, 25, 137–141.
4. Liu, Y., Tolentino, J., Gibbs, M., Ihly, R., Perkins, C. L., Liu, Y., Crawford, N., Hemminger, J. C. & Law, M. PbSe Quantum Dot Field-Effect Transistors with Air-Stable Electron Mobilities above $7 \text{ cm}^2 \text{ V}^{-1} \text{ s}^{-1}$. *Nano Lett.* **2013**, 1, 1578–1587.
5. Konstantatos, G., Howard, I., Fischer, A., Hoogland, S., Clifford, J., Klem, E., Levina, L. & Sargent, E. H. Ultrasensitive Solution-Cast Quantum Dot Photodetectors. *Nature* **2006**, 442, 180–183.
6. Werle, P., Slemr, F., Maurer, K., Kormann, R., Mucke, R. & Janker, B. Near- and Mid-Infrared Laser-Optical Sensors for Gas Analysis. *Opt. Las. Eng.* **2002**, 37, 101–114.
7. Rothman, L. S., Gordon, I. E., Barbe, A., Benner, D. C., Bernath, P. F., Birk, M., Boudon, V., Brown, L. R., Campargue, A., Champion, J.-P., Chance, K., Coudert, L. H., Dana, V., Devi, V. M., Fally, S., Flaud, J.-M., Gamache, R. R., Goldman, A., Jacquemart, D., Kleiner, I. *et al.* The HITRAN 2008 Molecular Spectroscopic Database. *J. Quant. Spectrosc. Radiat. Transf.* **2009**, 110, 533–572.